Available online at www.sciencedirect.com
SCIENCE DIRECT®
International Journal of Heat and Fluid Flow 25 (2004) 559–568
International Journal of HEAT AND FLUID FLOW
www.elsevier.com/locate/ijhff

Numerical simulation of magnetic control of heat transfer in thermal convection

S. Kenjereš *, K. Hanjalić

Department of Multi Scale Physics, Faculty of Applied Sciences, Delft University of Technology, Lorentzweg 1, 2628 CJ Delft, The Netherlands

Abstract

We report on numerical study of effects of orientation and distribution of an external magnetic field on the reorganization of convective structures and heat transfer in thermal convection in electrically conductive fluids. The simulations were performed using a transient RANS (T-RANS) approach in which the large-scale deterministic structures are numerically resolved in time and space and the unresolved contribution is modelled using an algebraic stress–flux three-equation subscale model. For low Prandtl (*Pr*) fluids the subscale model was extended to include *Pr*-dependent molecular dissipation of heat flux. The method was first validated in natural convection in a side-heated cubical enclosure subjected to magnetic fields of different orientation, strength and penetration depth, showing good agreement with the previous benchmark studies. Subsequently, a series of simulations was performed of turbulent Rayleigh–Bénard convection subjected to different magnetic fields over a range of Rayleigh (*Ra*) and Hartmann (*Ha*) numbers. The computed Nusselt number showed good agreement with the available experimental results. Numerical visualization of instantaneous flow patterns showed dramatic differences in the convective structures and local heat transfer for different orientation of the magnetic field with respect to the gravitation vector. A gradual, step-like increase in the magnetic strength revealed an interesting outcome of the "competition" between the buoyancy and the Lorentz forces, leading first to chaotic transition and eventually to laminarization. For specific ranges of *Ha*, it was found that a local magnetic field confined to the wall boundary layer along the thermally active walls provides almost equal effects as the homogeneous field over the whole flow, indicating an interesting possibility for controlling thermal convection and associated heat transfer.

Keywords: Numerical simulations; Thermal convection; Magnetic field; Heat transfer control; Turbulence

1. Introduction

The potential use of a magnetic field to control fluid flow and heat transfer in conductive fluids has long been recognized in many applications such as crystal growth, metal casting, liquid metal cooling blankets for fusion reactors, and others. A magnetic field imposed on electrically conducting fluid creates the Lorentz force in the plane perpendicular to the magnetic field vector, oriented in the direction opposite to the fluid velocity, thus retarding the motion perpendicular to the magnetic field. A number of numerical and experimental studies of thermal convection subjected to magnetic field of various orientation have been reported in the literature, but most deal with laminar flows (e.g. Ozoe and Okada, 1989; Mößner and Müller, 1999; Juel et al., 1999). Aurnou and Olson (2001) conducted a series of experiments dealing with Rayleigh–Bénard convection of liquid gallium in a large aspect ratio cavities (1:8 and 1:6) subjected to transversal magnetic field. The operative range of the experimental set-up was relatively small—covering $3 \times 10^3 \leqslant Ra \leqslant 1.6 \times 10^4$ regime, i.e. low turbulence regime appearing just after onset of thermal convection. Investigation of dependence of the critical Rayleigh number versus intensity of vertically oriented uniform magnetic field showed a good agreement with linear stability theory. Burr and Müller (2002) performed experimental and analytical studies of similar problem, but with the horizontally oriented uniform magnetic field. Their experiments again covered regimes close to the onset of thermal convection, i.e. $10^3 \leqslant Ra \leqslant 8 \times 10^4$. These experiments showed that the critical *Ra* number was shifted to significantly higher values due to magnetic breaking effects. In addition, these

* Corresponding author. Tel.: +31-15-278-3649; fax: +31-15-278-1204.
E-mail address: kenjeres@ws.tn.tudelft.nl (S. Kenjereš).

0142-727X/$ - see front matter © 2004 Elsevier Inc. All rights reserved.
doi:10.1016/j.ijheatfluidflow.2004.02.021

Nomenclature

L, H, D characteristic length, height and depth of domain (m)
$Ra = \beta g_i \Delta T Pr(\rho/\mu)^2 D^3$ Rayleigh number
$Nu = hD/\lambda$ Nusselt number
$Ha = B_0 L\sqrt{\sigma/\rho\nu}$ Hartmann number
$Re_t = \langle k\rangle^2/\nu\langle\varepsilon\rangle$ Reynolds turbulent number
$Pr = \nu/a$ Prandtl number
$\langle T\rangle$ temperature (K)
$\langle\Phi\rangle$ electric potential (V)
$\langle k\rangle$ turbulent kinetic energy (m^2/s^2)
$\langle\varepsilon\rangle$ dissipation rate of turbulent kinetic energy (m^2/s^3)
$\langle\theta^2\rangle$ temperature variance (K^2)
$\langle\varepsilon_\theta\rangle$ dissipation rate of temperature variance (K^2/s)
$\langle\varepsilon_{\theta i}\rangle$ heat flux dissipation ($m\,K/s^2$)
$\langle U_i\rangle$ velocity vector (m/s)
$\langle B_i\rangle$ magnetic field induction vector (T)
B_0 intensity of magnetic field (T)
$\mathbf{e}$ electric field intensity (V/m)
$\mathbf{j}$ electric current density (A/m^2)
τ_{ij} Reynolds stress (m^2/s^2)
$\tau_{\theta i}$ turbulent heat flux ($m\,K/s$)
ΔT wall temperature difference (K)
C_ϕ, $C_{\varepsilon_{\theta i}}$ constants in turbulence model

Greeks

ρ incompressible fluid density (kg/m^3)
ν kinematic viscosity (m^2/s)
ν_t turbulent viscosity
σ electric conductivity ($1/\Omega\,m$)
ξ, η constants in subscale (turbulence) model
ϵ_{ijk} unit tensor of third order

authors observed that the Nusselt number does not decrease monotonically with the increase in the intensity of the imposed magnetic field. An intermediate range is observed where the convective heat transfer locally increases before the final state of pure heat conduction is reached. This temporary increase in heat transfer was attributed to the reorganization of large-scale convective rolls aligned with the imposed magnetic field.

To our knowledge, no comparable works have been reported on the magnetoconvection in fully turbulent regime, although in many situations of practical relevance the flow is partially or fully turbulent. If the flow is turbulent, the imposed uniform magnetic field not only accelerates the decay of turbulence kinetic energy, but also causes a strong increase of turbulence anisotropy, Davidson (1997), because of tendency towards vortices elongation in the direction of the imposed magnetic field. The effect of the combined thermal buoyancy and Lorentz force on turbulence, and particularly on its structure morphology, depends on the mutual orientation between the two body forces. Capturing these effects at higher Re and Ra numbers and in complex geometries, which are beyond capability of direct numerical simulation (Rucklidge et al., 2000), requires to model the magnetic effects on turbulence either for the full spectrum as in RANS or at least for the subscale turbulence in LES and VLES approaches.

We consider different combinations, i.e. situations where the Lorentz force is aligned or perpendicular to the gravitational vector, both for a range of Ha and Ra numbers. The imposed magnetic fields are either homogeneously distributed over the whole flow domain, or locally confined to affect only the thin boundary layers along the thermally active walls.

2. Equations and the 'subscale' model

We have applied transient RANS approach (T-RANS) which was tested earlier in classical Rayleigh–Bénard convection over horizontal flat and wavy surfaces over a range of Ra numbers, $10^4 \leqslant Ra \leqslant 10^{15}$, all resulting in very good agreement with the available DNS and experimental results (Hanjalić and Kenjereš, 2001; Kenjereš and Hanjalić, 2002). This approach can be regarded as very large Eddy simulations (VLES) in which the unresolved random motion is modelled using a $\langle k\rangle$–$\langle\varepsilon\rangle$–$\langle\theta^2\rangle$ algebraic stress/flux single-point closure models, where $\langle\rangle$ denote the ensemble-averaged time-dependent variables (Kenjereš and Hanjalić, 1999). In contrast to LES, the contribution of both modes (resolved and subscale) to the turbulence second moments are of the same order of magnitude. The numerical method is then extended to include additional effects of magnetic fields making it possible to develop an integrated Navier–Stokes–Maxwell solver. Since we considered only the one-way coupling between fluid flow and electro-magnetic fluctuations (low magnetic Reynolds number assumption), the set of Maxwell equations reduces to solving only the equation for the electric potential $\langle\Phi\rangle$. For such systems, the set of equations describing the velocity and temperature fields and their coupling with the imposed electro-magnetic fields can be written as:

$$\frac{\partial\langle U_i\rangle}{\partial t}+\langle U_j\rangle\frac{\partial\langle U_i\rangle}{\partial x_j}=\frac{\partial}{\partial x_j}\left(\nu\frac{\partial\langle U_i\rangle}{\partial x_j}-\tau_{ij}\right)-\frac{1}{\rho}\frac{\partial(\langle P\rangle-P_{\mathrm{REF}})}{\partial x_i}+F_i^{\mathrm{T}} \tag{1}$$

$$\frac{\partial\langle T\rangle}{\partial t}+\langle U_j\rangle\frac{\partial\langle T\rangle}{\partial x_j}=\frac{\partial}{\partial x_j}\left(\frac{\nu}{Pr}\frac{\partial\langle T\rangle}{\partial x_j}-\tau_{\theta j}\right) \tag{2}$$

$$\nabla^2\langle\Phi\rangle=\nabla\cdot[\langle\mathbf{U}\rangle\times\langle\mathbf{B}\rangle] \tag{3}$$

$$\frac{D\langle k\rangle}{Dt}=\mathscr{D}_k+P_k+G_k^g+G_k^{\mathrm{L}}-\langle\varepsilon\rangle \tag{4}$$

$$\frac{D\langle\theta^2\rangle}{Dt}=\mathscr{D}_\theta+P_\theta-\langle\varepsilon_\theta\rangle \tag{5}$$

$$\frac{D\langle\varepsilon\rangle}{Dt}=\mathscr{D}_\varepsilon+P_{\varepsilon 1}+P_{\varepsilon 2}+G_\varepsilon^g+G_\varepsilon^{\mathrm{L}}-Y \tag{6}$$

where the F_i^{T} represents the total contribution of active body forces — here the thermal buoyancy and the Lorentz force:

$$F_i^{\mathrm{T}}=F_i^{\mathrm{B}}+F_i^{\mathrm{L}}=\beta g_i(\langle T\rangle-T_{\mathrm{REF}})+\frac{\sigma}{\rho}\left(-\epsilon_{ijk}\langle B_k\rangle\frac{\partial\langle\Phi\rangle}{\partial x_j}+\langle U_k\rangle\langle B_i\rangle\langle B_k\rangle-\langle U_i\rangle\langle B_k^2\rangle\right) \tag{7}$$

The direct influence of the magnetic field on turbulence is taken into account by additional terms in the equations for the subscale turbulence kinetic energy $\langle k\rangle$ and its dissipation rate $\langle\varepsilon\rangle$ (Kenjereš and Hanjalić, 2000a):

$$G_k^{\mathrm{L}}=-\frac{\sigma}{\rho}B_0^2\langle k\rangle\exp\left(-C_L\frac{\sigma}{\rho}B_0^2\frac{\langle k\rangle}{\langle\varepsilon\rangle}\right),\quad G_\varepsilon^{\mathrm{L}}=C_{\varepsilon 4}G_k^{\mathrm{L}}\frac{\langle\varepsilon\rangle}{\langle k\rangle} \tag{8}$$

with $C_L=0.025$ and $C_{\varepsilon 4}=1$. Here, σ and ρ are the electric conductivity and density of the fluid, respectively. The subscale contribution to the turbulent heat flux is expressed in the following form:

$$\tau_{\theta i}=-C_\phi\frac{\langle k\rangle}{\langle\varepsilon\rangle}\left[\tau_{ij}\frac{\partial\langle T\rangle}{\partial x_j}+\xi\tau_{\theta j}\frac{\partial\langle U_i\rangle}{\partial x_j}+\eta\big(\beta g_i\langle\theta^2\rangle+\langle\theta f_i^{\mathrm{L}}\rangle\big)+\langle\varepsilon_{\theta i}\rangle\right] \tag{9}$$

with

$$f_i^{\mathrm{L}}=\mathbf{j}\times\mathbf{B}=\frac{\sigma}{\rho}(\underbrace{-\nabla\phi_e}_{\mathbf{e}}+\mathbf{u}\times\mathbf{B})\times\mathbf{B},$$

$$\langle\varepsilon_{\theta i}\rangle=f_{\varepsilon_{\theta i}}\frac{1+Pr}{2\sqrt{PrR}}\frac{\langle\varepsilon\rangle}{\langle k\rangle}\tau_{\theta i} \tag{10}$$

where f_i^{L} is the fluctuating Lorentz force, $\mathbf{j}$ is the fluctuating total electric current, $\mathbf{e}$ is the fluctuating electric field, ϕ_e is the fluctuating electric potential, $\langle\varepsilon_{\theta i}\rangle$ is the molecular heat flux dissipation and R is the time scale ratio ($R=\tau_\theta/\tau_{\mathrm{m}}=0.5$). The detailed specification of all terms and the model coefficients can be found in Kenjereš and Hanjalić (2000b).

3. Solution method

The equation set is solved using a finite-volume Navier–Stokes–Maxwell solver for three-dimensional flows in structured non-orthogonal geometries. The solver can be run in serial (single processor) or parallel mode utilizing the domain decomposition MPI directives. The Cartesian vectors and tensors components in the collocated arrangement are applied for all variables. The second-order central difference scheme (CDS) is applied for the discretization of diffusive terms in all equations and of convective terms in the $\langle U,V,W,T,\Phi\rangle$ equations. The second-order linear upwind scheme (LUDS) is applied for convective terms in the equations of subscale turbulent contributions, i.e. $\langle k,\varepsilon,\theta^2\rangle$. The time integration is performed by fully implicit second-order three-time-level method which allows larger time steps to be used as compared to explicit marching schemes.

4. Results and discussion

4.1. Side-heated cubical enclosure subjected to magnetic fields: laminar and transitional regimes

In order to validate the recently developed combined Navier–Stokes–Maxwell solver, first we performed three-dimensional numerical computations of magnetic laminar and transitional convection ($Ra=10^6$, $Pr=0.054$) in electrically insulated cubical enclosure with side-heating and cooling and with different orientations of an imposed uniform magnetic field. The comparison with similar simulations of Ozoe and Okada (1989), Mößner and Müller (1999) and Juel et al. (1999) gave generally good agreement. We observed that the maximum reduction in heat transfer is achieved when the magnetic field is imposed in the horizontal x-direction ($\mathbf{B}\|x$), aligned with the mean temperature gradient (Fig. 1). For the horizontal spanwise orientation of the magnetic field, ($\mathbf{B}\|y$), only small changes in the reorganization of the flow structures are observed compared to the situations when the magnetic field is switched off (Fig. 2). Consequently, very modest reductions of Nu are obtained even for the high values of Ha.

In addition to the homogeneously applied magnetic fields along the main coordinate directions (as it was done in the previous studies), we also applied locally confined magnetic field which influences only the boundary layers along the thermally active walls. Here

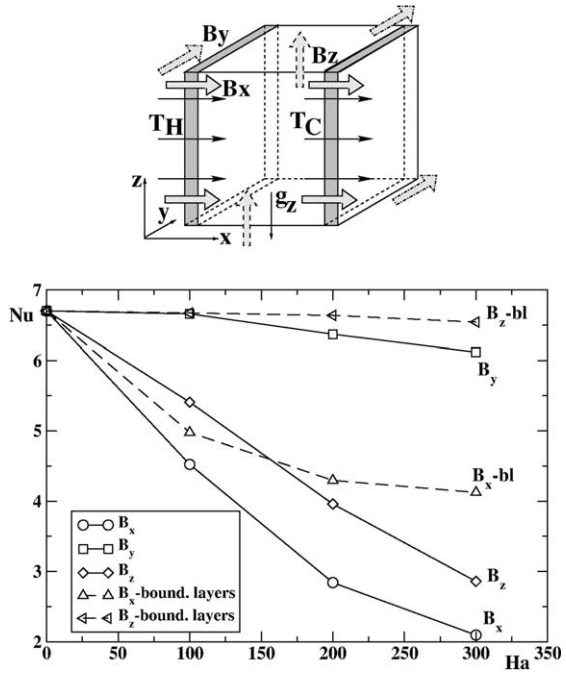

Fig. 1. Reduction in the integral heat transfer coefficient for a side-heated cubical cavity subjected to external magnetic fields of different orientation (B_x, B_y and B_z) distributed homogeneously or confined only to boundary layers along the thermally active vertical walls (B_x^{bl}, B_z^{bl}): $Ra = 10^6$, $Pr = 0.054$, $0 \leqslant Ha \leqslant 300$.

the magnetic field is active only in the near-wall region up to the distance where the vertical velocity reaches its maximum in the situation when the magnetic field is switched off. The orientations of the magnetic fields are chosen to be in the x- and z-directions since these orientations showed to be most efficient in damping the heat transfer. A strong reduction in heat transfer is again observed for $\mathbf{B}\|x$ orientation. This damping of heat transfer for $0 \leqslant Ha \leqslant 150$ is even more efficient than $\mathbf{B}\|z$ orientation applied over the whole fluid. For $Ha \geqslant 200$ a further increase in the intensity of the magnetic field does not bring any significant reduction in Nu, i.e. a sort of an asymptotic state is approached. It is noted that this boundary-layer-confined magnetic field produced very significant reduction in heat transfer—about 40%. Such confined magnetic fields can easily be generated in practical applications and are considered as an attractive means for suppressing heat transfer. Note that a non-uniform mesh with 82^3 and 102^3 control cells clustered towards the walls has been applied for the homogeneously and partially imposed magnetic fields, respectively, ensuring in both cases that the Hartmann boundary layers ($\delta_H \propto 1/Ha$) are well resolved for all values of Ha.

It is interesting to look into the physical origin of the specific alignments which lead to the most efficient suppression of fluid flow and, consequently, to the most efficient reduction in the integral heat transfer. The key

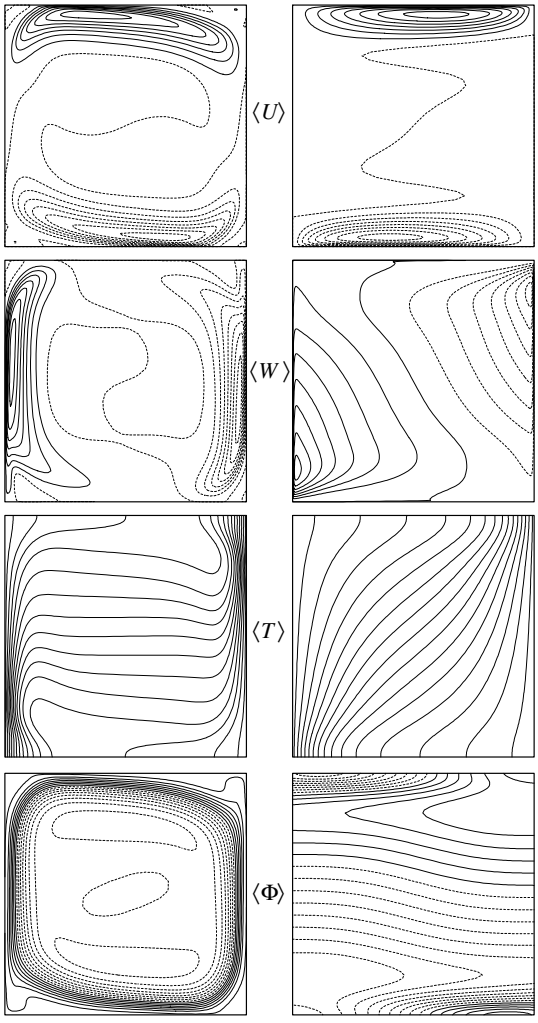

Fig. 2. Reorganization of the flow pattern, temperature and electric potential fields in the central vertical (x–z) plane of a cubical cavity for different orientation of magnetic fields at $Ra = 10^6$, $Pr = 0.054$. Left: $\mathbf{B}\|y$, $Ha = 100$, $\langle U\rangle_{\min}^{\max} = \pm 0.5$, $\langle W\rangle_{\min}^{\max} = \pm 0.55$, $\langle \Phi\rangle_{\min}^{\max} = \pm 2 \times 10^{-2}$; right: $\mathbf{B}\|x$, $Ha = 300$, $\langle U\rangle_{\min}^{\max} = \pm 0.1$, $\langle W\rangle_{\min}^{\max} = \pm 0.05$, $\langle \Phi\rangle_{\min}^{\max} = \pm 2 \times 10^{-4}$, $0 \leqslant \langle T\rangle \leqslant 1$.

is in the specific distribution of the electro-magnetic parameters, i.e. electric currents and the resulting electric potential. By comparing the $\mathbf{B}\|x$ and $\mathbf{B}\|y$ alignments, the expressions for the Lorentz force components in the vertical direction can be written as $F_z^L = -\sigma/\rho B_x(-\partial\Phi/\partial y + W \cdot B_x)$ and $F_z^L = \sigma/\rho B_y(-\partial\Phi/\partial x - W \cdot B_y)$, respectively. It can be seen that the $\partial\Phi/\partial x$ contribution is much higher than $\partial\Phi/\partial y$ (electric potential distributions shown in Fig. 2). This dominant term is counterbalanced by the $W \cdot B_y$ product, and as a result, the total F_z^L contribution is very small for $\mathbf{B}\|y$ orientation. Because of the small value of the Lorentz force, the suppression of the fluid motion is negligible and consequently, no significant reduction in heat transfer is observed. These findings are in full accordance with the analysis performed by Ozoe and Okada (1989).

4.2. Accounting for low Prandtl numbers

In our previous studies, Hanjalić and Kenjereš (2000, 2001), we presented a three-equations $\langle k\rangle$–$\langle\varepsilon\rangle$–$\langle\theta^2\rangle$ ASM/AFM model for turbulent flows subjected simultaneously to thermal buoyancy and Lorentz force, but we considered only the fluids with the Prandtl number close to unity. Here we focus on liquid metals and introduce additional low-*Pr* modifications. In a series of direct numerical simulation (DNS) of RB and internally heated convection with liquid metals ($Pr = 0.006, 0.025$), Wörner and Grötzbach (1995) showed that the molecular destruction $\langle\varepsilon_{\theta i}\rangle$ was the main sink in the turbulent heat flux equation instead of the pressure-scrambling contribution. Hanjalić (1994) proposed a model for the molecular dissipation of $\langle\tau_{\theta i}\rangle$ in RANS computations, here written for the subscale model, as:

$$\langle\varepsilon_{\theta i}\rangle = f_{\varepsilon_{\theta i}} \frac{1}{\sqrt{2R}} \frac{\langle\varepsilon\rangle}{\langle k\rangle} \tau_{\theta i} \tag{11}$$

where $f_{\varepsilon_{\theta i}}$ should be a function of the turbulent Péclet turbulent number ($Pe_t = \langle k\rangle^2/a\langle\varepsilon\rangle$). Wörner and Grötzbach (1995) a priori tested this form of model using their DNS results and concluded that a correction to account for the effects of low-*Pr* number is needed. They proposed a simplified version of the Shikazono and Kasagi (1996) model in the following form:

$$\langle\varepsilon_{\theta i}\rangle = f_{\varepsilon_{\theta i}} \frac{1+Pr}{2\sqrt{PrR}} \frac{\langle\varepsilon\rangle}{\langle k\rangle} \tau_{\theta i} \tag{12}$$

with

$$f_{\varepsilon_{\theta i}} = \exp[-C_{\varepsilon_{\theta i}} Re_t (1+Pr)] \tag{13}$$

where $Re_t = \langle k\rangle^2/\nu\langle\varepsilon\rangle$ is the turbulent Reynolds number and $C_{\varepsilon_{\theta i}} = 7\times10^{-4}$. We applied this model to the computation of the classic low-*Pr* turbulent Rayleigh–Bénard (RB) convection and compared results with recent DNS of Kerr and Herring (2000), $10^4 \leqslant Ra \leqslant 2\times10^6$, $Pr = 0.07$. It can be seen that the inclusion of the $\langle\varepsilon_{\theta i}\rangle$ into $\tau_{\theta i}$ provided *Nu* in excellent agreement with DNS over the entire range of *Ra* (Fig. 3). It is noted that the computational mesh $82\times82\times72$ used here for the T-RANS over a range of *Ra* numbers up to 2×10^6 is much coarser than a typical DNS mesh: for example, it contains only 5% of the total number of grid points of the $256\times256\times128$ DNS mesh used by Kerr and Herring (2000) for $Ra = 2\times10^6$ (their highest simulated *Ra*).

4.3. Turbulent Rayleigh–Bénard convection in different magnetic fields

We consider next the Rayleigh–Bénard convection subjected to external magnetic fields of different orientations over a range of *Ra* ($10^7 \leqslant Ra \leqslant 10^9$) and *Ha* ($0 \leqslant Ha \leqslant 500$) numbers. We investigated again the homogeneously distributed magnetic fields imposed

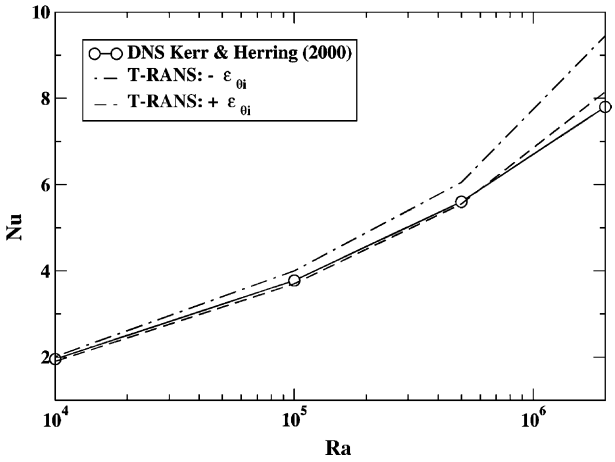

Fig. 3. Effect of inclusion of the molecular heat flux dissipation $\langle\varepsilon_{\theta i}\rangle$ into subscale representation of the turbulent heat flux $\tau_{\theta i}$: comparison with DNS results of Kerr and Herring (2000), $10^4 \leqslant Ra \leqslant 2\times10^6$, $Pr = 0.07$.

over the entire cavity height, as well as local magnetic fields confined just to the near-wall regions. The simulation domain of 1:8 aspect ratio has been discretized by a computational mesh uniform in the horizontal directions but clustered close to the walls in the vertical direction. When a locally confined magnetic field is applied, the mesh is additionally clustered in the near-wall region in order to resolve the gradients of the magnetic field in the vertical direction. In both situations the total mesh is represented by 82×82 control volumes (CV) in the horizontal and by 72 CVs in the vertical direction for the magnetic field over the entire cavity height, or 82 CVs for the magnetic field confined to the near-wall region. The typical values of the non-dimensional time step $\Delta\tau = \Delta t/\sqrt{\beta g\,\Delta T/H}$ varied between 0.01 for lower *Ra*'s and 0.0025 for higher *Ra*'s.

The effect of a transversal magnetic field ($\mathbf{B}\|z$) on the integral heat transfer (*Nu*) for all simulated situations is shown in Fig. 4. Here, the Nu_0 is the value of *Nu* for the neutral situation ($Ha = 0$) and the Nu_B is the value of *Nu* when the magnetic field is active. Good agreement between the present simulations and the experimental results of Cioni et al. (2000) has been obtained despite the difference in geometries considered: the experiments were performed in a vertical cylinder with aspect ratio $D/H = 1$ where one can expect more intensive convection compared to the classical RB between infinite walls. It is noted that for all *Ra* numbers considered, the flow will be highly turbulent in the absence of the magnetic field. As expected, very significant reduction in heat transfer is observed. With this orientation of the magnetic field, it is even possible to totally suppress any convective motion and to produce pure diffusive regime.

This effect can be easily explained by the fact that the vertically oriented magnetic field creates the Lorentz force that acts in the horizontal plane and suppresses

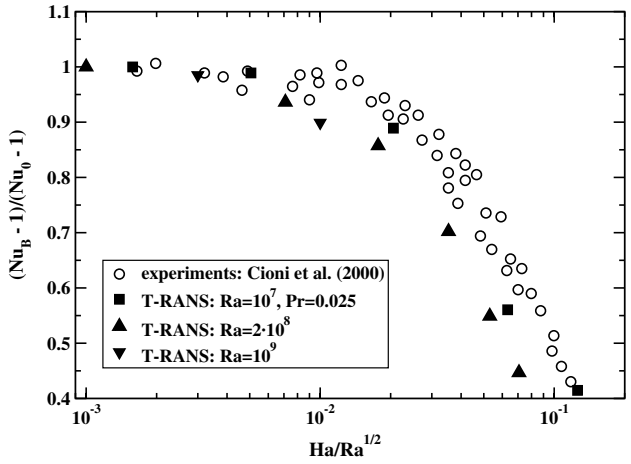

Fig. 4. Reduction in the integral heat transfer coefficient for highly turbulent Rayleigh–Bénard convection subjected to a vertical magnetic field of different intensity $10^7 \leqslant Ra \leqslant 10^9$, $0 < Ha \leqslant 500$, $Pr = 0.025$—comparison with experimental results of Cioni et al. (2000).

horizontal motion creating vertically elongated almost-cylindrical convective cell pattern, with very thin thermal plumes in between (Fig. 5). With an increase in the intensity of the magnetic field these structures are 'squeezed' further until they break suppressing thus entirely the convective motion.

The reorganization of the vertical velocity $\langle W \rangle$ and the temperature $\langle T \rangle$ in the central vertical plane for different orientations of the magnetic field is illustrated in Fig. 6. For the $\mathbf{B}\|z$ situation where the magnetic field is locally confined to the near-wall regions ($0 \leqslant z/D \leqslant 0.005$, $0.95 \leqslant z/D \leqslant 1$), the structure gets detached from the wall boundary layers, levitating freely in the core region. The locally applied magnetic field near the walls almost totally suppresses the velocity and its fluctuations in this region, creating conductive-like buffer with almost linear distribution of the temperature field (Fig. 6-middle). This finding can be of use for controlling heat transfer in various applications, such as future generation of advanced fusion reactors (Satake et al., 2002). In addition, in the central zone the temperature contours show less pronounced gradients indicating better mixing. With the longitudinal orientation of a homogeneously distributed magnetic field ($\mathbf{B}\|y$) a significantly different picture is obtained (Fig. 6-bottom). Very regular, two-dimensional morphology of velocity and temperature field is observed. This is in accordance with our expectations since this configuration should produce structures elongated in the direction of the applied magnetic field. It is interesting to notice the additional small cells nested just below/above the large rolls with rotation in the opposite direction (Fig. 6-bottom).

In order to illustrate quantitatively the effects of flow structure reorganizations on the integral heat transfer (for this specific value of $Ra = 10^7$), we show in Fig. 7

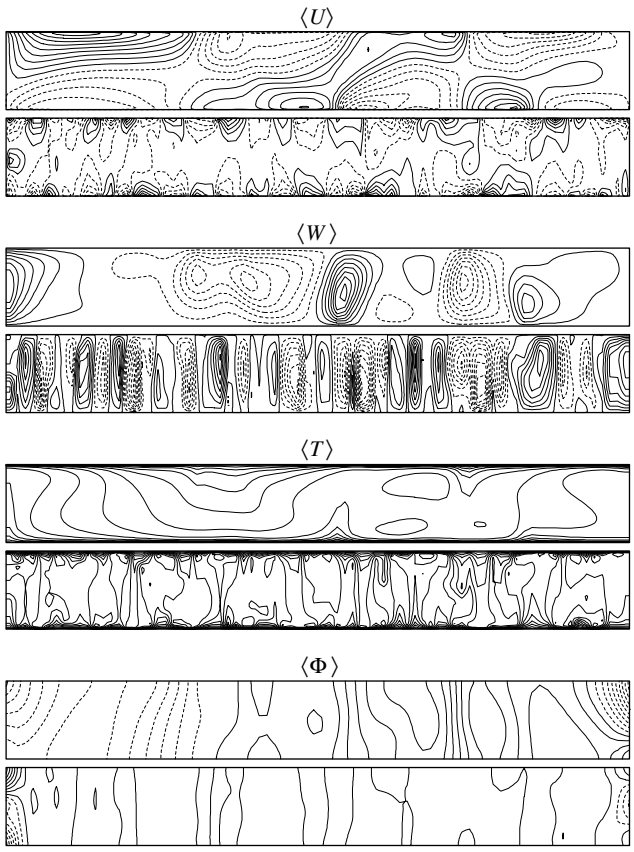

Fig. 5. Rayleigh–Bénard turbulent convection at $Ra = 2 \times 10^8$, $Pr = 0.025$, subjected to a vertically oriented magnetic field; from above to below: distribution of instantaneous horizontal velocity $\langle U \rangle$, vertical velocity $\langle W \rangle$, temperature $\langle T \rangle$ and electric potential $\langle \Phi \rangle$ in the central vertical cross-section. First: $Ha = 100$, $\langle U \rangle_{\min}^{\max} = \pm 0.3$, $\langle W \rangle_{\min}^{\max} = \pm 0.3$, $\langle \Phi \rangle_{\min}^{\max} = \pm 0.1$; second: $Ha = 500$, $\langle U \rangle_{\min}^{\max} = \pm 0.15$, $\langle W \rangle_{\min}^{\max} = \pm 0.3$, $\langle \Phi \rangle_{\min}^{\max} = \pm 0.01$. For all cases $0 \leqslant \langle T \rangle \leqslant 1$.

the Nu dependence on Ha. It has already been mentioned that for a homogeneously distributed magnetic field, the $\mathbf{B}\|z$ orientation can lead to a pure diffusive regime. In contrast to this situation, the $\mathbf{B}\|y$ orientation reduces significantly heat transfer only up to the condition when the fully two-dimensional state is obtained. After this point, additional increase in the magnetic field intensity will bring no further heat transfer reduction. A comparison of Nu–Ha dependence for different situations reveals some interesting phenomena. For the weak magnetic fields, $15 \leqslant Ha \leqslant 65$, the $\mathbf{B}\|y$ orientation resulted in the weakest heat transfer reduction. In the $65 \leqslant Ha \leqslant 200$ interval, due to very dramatic flow reorganization towards the two-dimensional state, heat transfer is reduced much more efficiently than in the case of partially confined $\mathbf{B}\|z$ orientation. In the same interval, a very strong damping of Nu occurs for the locally confined $\mathbf{B}\|z$ orientation. It can be concluded for all situations considered that the $Nu(Ha)$ behavior is non-monotonic. This finding stresses the importance of and the need for optimizing the distributions of the

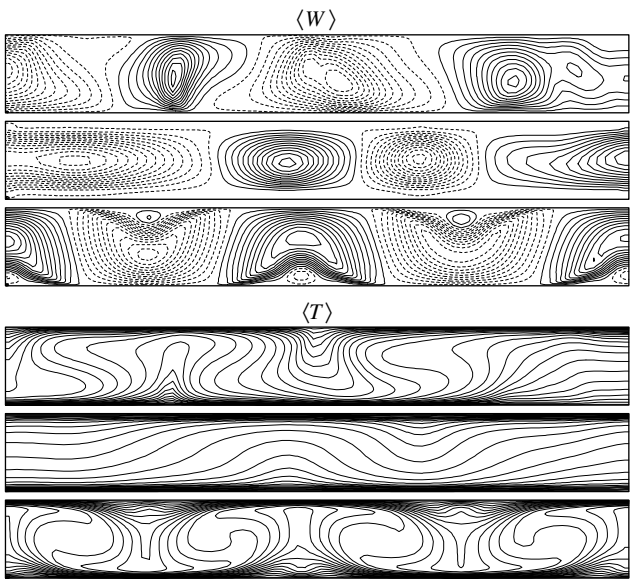

Fig. 6. Turbulent Rayleigh–Bénard convection at $Ra = 10^7$, $Pr = 0.025$, subjected to external magnetic fields of different orientation and strength. First: $Ha = 0$, $\langle W\rangle_{\min}^{\max} = \pm 0.3$; second: $Ha = 500$ vertical magnetic field applied in the near-wall region $0 \leqslant z/D < 0.05$ and $0.95 \leqslant z/D < 1$, $\langle W\rangle_{\min}^{\max} = \pm 0.3$; third: longitudinal magnetic field, $Ha = 500$, $\langle W\rangle_{\min}^{\max} = \pm 0.325$, $0 \leqslant \langle T\rangle \leqslant 1$ for all cases.

imposed magnetic field and its orientation with respect to the gravitational vector in order to achieve the desired control of heat transfer.

A further illustration of the flow reorganization due to an imposed magnetic field is given by plots of the contours of the instantaneous vertical velocity and temperature in the central horizontal plane (Figs. 8 and 9). Compared to the neutral situation ($Ha = 0$), both $\mathbf{B}\|z$ and $\mathbf{B}\|y$ orientations at $Ha = 200$ produced dramatic changes in flow and temperature fields. In principle, two basic trends can be seen: the $\mathbf{B}\|z$ orientation

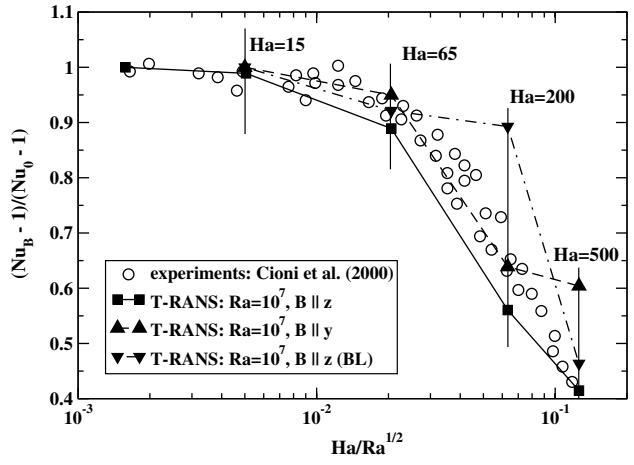

Fig. 7. Effects of different magnetic field orientations on integral heat transfer, $Ra = 10^7$, $Pr = 0.025$.

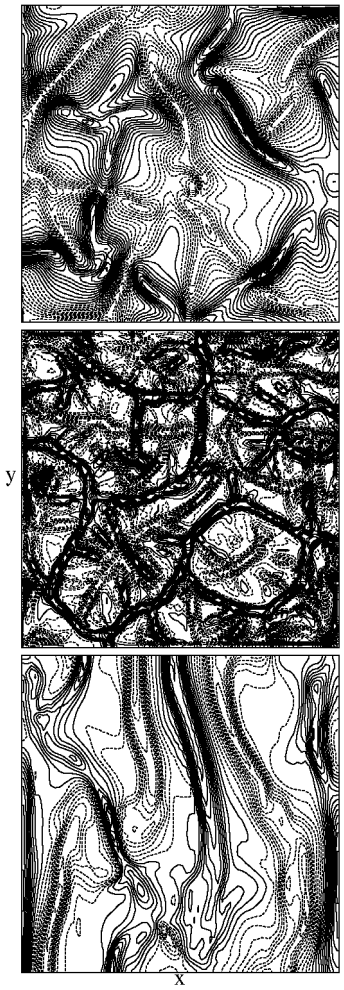

Fig. 8. Vertical velocity $\langle W\rangle$ distribution in the central horizontal (x–y) plane ($z/D = 0.5$), $Ra = 10^7$, $Pr = 0.025$. Above: $Ha = 0$, no magnetic field, $\langle W\rangle_{\min}^{\max} = \pm 0.4$; middle: $Ha = 200$, transversal magnetic field ($\mathbf{B}\|z$), $\langle W\rangle_{\min}^{\max} = \pm 0.45$; below: $Ha = 200$, longitudinal magnetic field ($\mathbf{B}\|y$), $\langle W\rangle_{\min}^{\max} = \pm 0.55$.

tends to produce more dense structures (suppression of the convective structures) and the $\mathbf{B}\|y$ orientation tends to impose two-dimensional alignments in the y-direction. The imprints of the underlying thermal plumes and of the produced updrafts and downdrafts can be seen in Fig. 8. Here, the contours of positive or negative values of $\langle W\rangle$ are plotted with solid and dashed lines respectively. As expected, very close resemblance between the thermal and velocity field is observed (Fig. 9).

A summary of the local distributions of Nu at the hot wall for the considered test cases is shown in Fig. 10. It is interesting to observe that the $\mathbf{B}\|z$ orientation can produce larger local values of Nu compared to the neutral situations ($Ha = 0$) despite the fact that the integral heat transfer is reduced. This can be explained by more intensive penetrative capabilities of the vertically elongated nearly cylindrical thermal plumes with more concentrated vertical momentum and vertical heat flux.

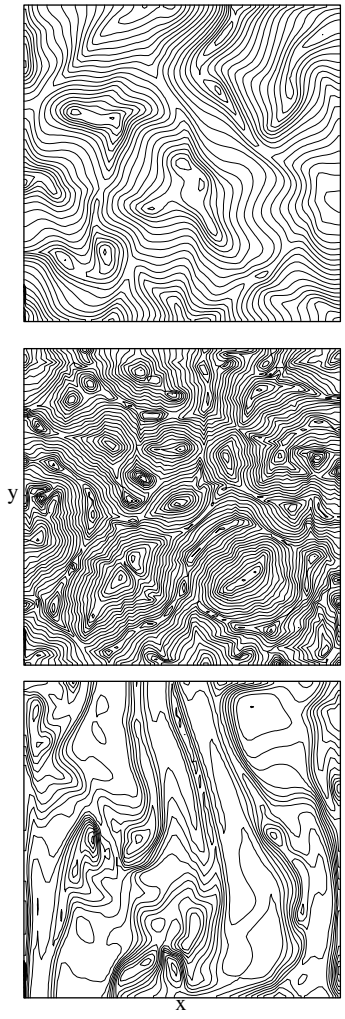

Fig. 9. Temperature $\langle T\rangle$ distribution in the central horizontal (x–y) plane ($z/D = 0.5$): see caption in the previous figure (contours of temperature $0 \leqslant \langle T\rangle \leqslant 1$ uniformly distributed).

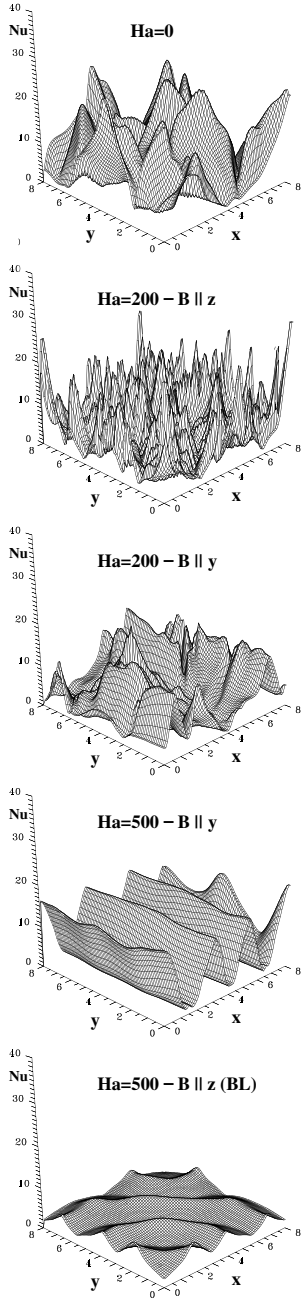

Fig. 10. Distributions of the local Nusselt number on the hot wall for different orientations, distributions and intensities of the external magnetic field: $Ra = 10^7$, $Pr = 0.025$.

This leads to the local thinning of the thermal boundary layers on the horizontal walls and higher local temperature gradients at the wall. The effects of the $\mathbf{B}\|y$ orientation show gradually appearing alignment with the y-axis. For the most intensive magnetic field applied ($Ha = 500$), very regular two-dimensional sinusoidal distributions is obtained. It is already mentioned that the locally confined $\mathbf{B}\|z$ orientation produced very rapid damping of Nu. At the same time a quite uniform distribution of the local Nu is produced.

4.4. Dynamics of magnetic laminarization

The time evolution of the Nusselt numbers and of the maximal velocity components with gradually increasing intensity of a vertically imposed magnetic field for $Ra = 10^7$ and $Pr = 0.025$ are shown in Fig. 11. First, the simulation was performed for neutral conditions without magnetic field for the time period $0 \leqslant t \leqslant 480$ in order to obtain fully developed turbulent thermal convection. Then, in order to investigate the time response of the heat transfer to the imposed magnetic field, a vertically oriented uniform magnetic field is activated. Its intensity is gradually increased in intervals of $\Delta Ha = 50$ and kept constant over periods of 30 non-dimensional time units. It is interesting to observe that for each new interval of the ΔHa increase, a significant drop of Nu is observed (Fig. 11-above). It takes about 5 (for $Ha = 100$, $515 \leqslant t \leqslant 545$) to even 15

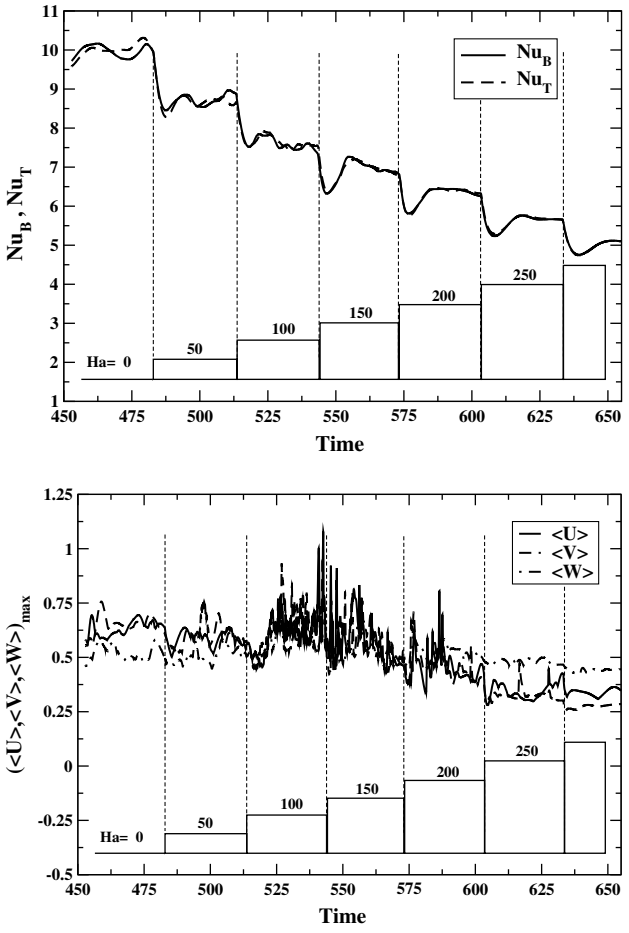

Fig. 11. Time evolution of the Nusselt numbers on the top and bottom wall (above) and maximal velocity components (below) for a vertically imposed magnetic field which intensity is gradually increased by $\Delta Ha = 50$ and kept over intervals of 30 non-dimensional time units, $Ra = 10^7$, $Pr = 0.025$, $Ha = 0, \ldots, 300$.

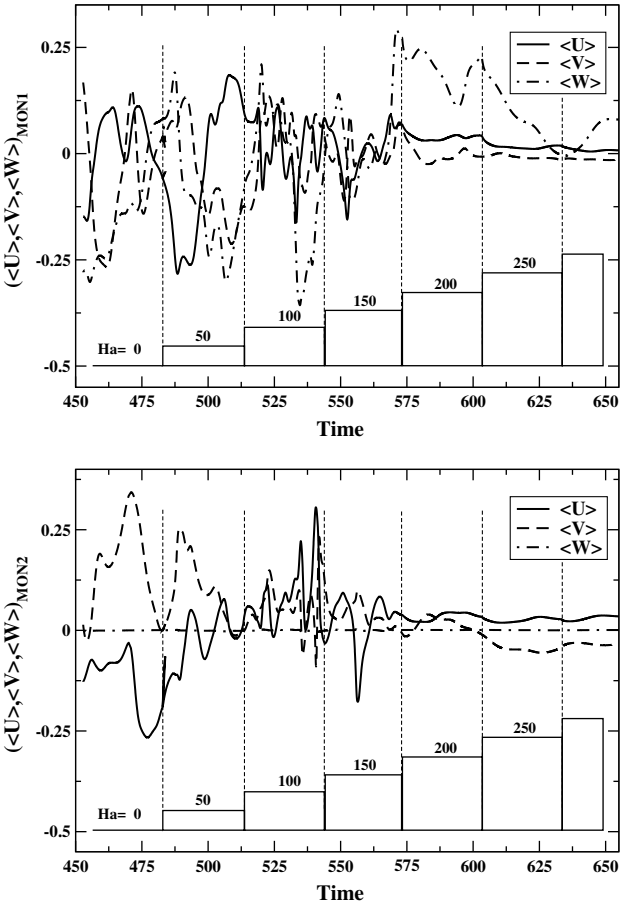

Fig. 12. Time evolution of velocity components at characteristic monitoring locations: $x/L = 0.5$, $y/H = 0.5$, $z/D = 0.5$ (above), and $x/L = 0.5$, $y/H = 0.5$, $z/D = 0.95$ (below), for identical conditions as in Fig. 11.

(for $Ha = 300$, $630 \leqslant t \leqslant 660$) additional time-units to reach a relatively stabile regime of heat transfer. Finally, for $Ha = 300$ a reduction of about 50% in the integral heat transfer is achieved, compared to the neutral case. The time evolution of the maximal velocity components (over the entire domain) for the corresponding situations is shown in Fig. 11-below. This time evolution can be clearly divided into three characteristic intervals. The first interval shows a highly turbulent regime, still not significantly affected by the imposed magnetic field, $t \leqslant 515$. After an additional increase in the magnetic field intensity, a strong competition between the thermal buoyancy (gravitational field) and the Lorentz force takes place, resulting in a significant increase in velocity components, $515 \leqslant t \leqslant 550$. This increase is particularly intensive for the horizontal velocity components, i.e. $\langle U, V \rangle$. After this transition interval, $t \geqslant 600$, a more quiet period appears—characterized by significantly reduced values in the horizontal velocity components. This is an indication that the Lorentz force is taking over the thermal buoyancy and that the horizontal movement of thermal plumes is significantly reduced. Similar intervals can be observed by analyzing the time evolution of velocity components at the characteristic monitoring points (Fig. 12). The first monitoring point is located in the center of the domain, $x/L = 0.5$, $y/H = 0.5$, $z/D = 0.5$ and the second point is located close to the bottom wall, $x/L = 0.5$, $y/H = 0.5$, $z/D = 0.95$. Here we focus on the time interval where the Lorentz force is dominant, i.e. $t \geqslant 575$. It can be seen that for higher intensities of the magnetic field, all velocity components are significantly reduced at both monitoring locations. Because the Lorentz force acts in the horizontal plane, the horizontal velocity components are much more reduced compared to the vertical component at the monitoring location at the center (Fig. 12-above). Close to the bottom wall, the vertical component is strongly suppressed due to the wall vicinity, but the remaining velocity components also show a significant reduction both in amplitudes and in total intensity (Fig. 12-below).

5. Conclusions

The time-dependent Reynolds-averaged Navier–Stokes method (T-RANS), tested earlier in various flows dominated by large scale deterministic structures, was applied to study effects of different distribution and orientation of an imposed magnetic field on flow and heat transfer in thermal convection. Two configurations were considered: a side-heated cavity and Rayleigh–Bénard convection, both for a range of *Ra* and *Ha* numbers. The computed convective structures and Nusselt number distribution on the bounding walls reveal very different effects of the imposed magnetic field depending on its orientation and distribution. For a side-heated cavity, the horizontal magnetic field ($\mathbf{B}\|x$) aligned with the mean temperature gradient (∇T) produces a drastic heat transfer damping, whereas the spanwise horizontal field ($\mathbf{B}\|y$, perpendicular to ∇T) causes hardly any changes. In the case of RB convection, a vertical homogeneous magnetic field causes a strong reduction in both the integral and local heat transfer coefficients, while in a spanwise field the effect is weaker.

The application of a local wall-normal magnetic field, confined to the near-wall region, proved in both configurations to be almost equally effective as the homogeneous field over the entire flow, especially for lower magnetic intensities. Because a local magnetic field in the near-wall region can easily be generated in practical situations, this finding opens an interesting potential for controlling heat transfer in thermal convection. However, because the $Nu(Ha)$ behavior in some configurations is not monotonic, the distribution and orientation of the imposed magnetic field needs to be optimized for each specific application.

The T-RANS approach was demonstrated to be a credible tool for optimization of magnetic field to control heat transfer in various applications.

Acknowledgements

The research of Dr. Saša Kenjereš has been made possible by a fellowship of the Royal Netherlands Academy of Arts and Sciences (KNAW).

References

Aurnou, J.M., Olson, P.L., 2001. Experiments on Rayleigh–Bénard convection, magnetoconvection and rotating magnetoconvection in liquid gallium. J. Fluid Mech. 430, 283–307.

Burr, U., Müller, U., 2002. Rayleigh–Bénard convection in liquid metal layers under the influence of a horizontal magnetic field. J. Fluid Mech. 453, 345–369.

Cioni, S.S., Chaumat, S., Sommeria, J., 2000. Effect of a vertical magnetic field on turbulent Rayleigh–Bénard convection. Phys. Rev. E 62 (4), R4520–R4523, Part A.

Davidson, P.A., 1997. The role of angular momentum in the magnetic damping of turbulence. J. Fluid Mech. 336, 123–150.

Hanjalić, K., 1994. Achievements and limitations in modeling and computation of buoyant turbulent flows and heat transfer. In: Invited Keynote Lecture, Proceedings of the 10th International Heat Transfer Conference, Brighton, UK, Vol. 1, pp. 1–18.

Hanjalić, K., Kenjereš, S., 2000. Reorganization of turbulence structure in magnetic Rayleigh–Benard convection: a T-RANS study. J. Turbul. 1 (8), 1–22.

Hanjalić, K., Kenjereš, S., 2001. 'T-RANS' simulation of deterministic eddy structure in flows driven by thermal buoyancy and Lorentz force. Flow Turbul. Combust. 66 (4), 427–451.

Juel, A., Mullin, T., Ben Hadid, H., Henry, D., 1999. Magnetohydrodynamic convection in molten gallium. J. Fluid Mech. 378, 97–118.

Kenjereš, S., Hanjalić, K., 1999. Transient analysis of Rayleigh–Benard convection with a RANS model. Int. J. Heat Fluid Flow 20 (3), 329–340.

Kenjereš, S., Hanjalić, K., 2000a. On the implementation of effects of Lorentz force in turbulence closure models. Int. J. Heat Fluid Flow 21 (3), 329–337.

Kenjereš, S., Hanjalić, K., 2000b. Convective rolls and heat transfer in finite-length Rayleigh–Bénard convection: a two-dimensional numerical study. Phys. Rev. E 62 (6), 7987–7998.

Kenjereš, S., Hanjalić, K., 2002. Numerical insight into flow structure in ultraturbulent thermal convection. Phys. Rev. E 66 (3), art. no. 036307, Part 2B, pp. 1–5.

Kerr, R.M., Herring, J.R., 2000. Prandtl number dependence of Nusselt number in direct numerical simulations. J. Fluid Mech. 419, 325–344.

Mößner, R., Müller, U., 1999. A numerical investigation of three-dimensional magnetoconvection in rectangular cavities. Int. J. Heat Mass Transfer 42 (6), 1111–1121.

Ozoe, H., Okada, K., 1989. The effect of the direction of the external magnetic-field on the three-dimensional natural convection in a cubical enclosure. Int. J. Heat Mass Transfer 32 (10), 1939–1954.

Rucklidge, A.M., Weiss, N.O., Brownjoh, D.P., Matthews, P.C., Proctor, M.R.E., 2000. Compressible magnetoconvection in three dimensions: pattern formation in a strongly stratified layer. J. Fluid Mech. 419, 283–323.

Satake, S., Kunugi, T., Smolentsev, S., 2002. Advances in direct numerical simulation for MHD modeling of free surface flows. Fusion Eng. Des. 61 (2), 95–102.

Shikazono, N., Kasagi, N., 1996. Second-moment closure for turbulent scalar transport at various Prandtl numbers. Int. J. Heat Mass Transfer 39 (4), 2972–2987.

Wörner, M., Grötzbach, G., 1995. Modelling the molecular terms in the turbulent heat flux equation for natural convection. In: Proceedings of the 10th Symposium on Turbulent Shear Flows, Pennsylvania State University, State College, USA, Vol. 2, pp. 73–78.